Journal of Industrial and Management Optimization

https://www.aimspress.com/journal/jimo

JIMO, 22(6): 2912–2941.
DOI:10.3934/jimo.2026107
Received: 09 February 2026
Revised: 04 May 2026
Accepted: 14 May 2026
Published: 26 May 2026

Research article

Systemic resilience in heterogeneous supply chains: optimal targeted interventions against risk contagion

Shufen Wei[1], Yannan Su[2,*], Zhanyu Wang[1], Xinze Lian[3] and Feng Rao[1,*]

[1] School of Physical and Mathematical Sciences, Nanjing Tech University, Nanjing, Jiangsu 211816, China

[2] Nanjing Securities Co., Ltd. 389 Jiangdong Middle Road, Nanjing, Jiangsu 220019, China

[3] School of Data Science and Artificial Intelligence, Wenzhou University of Technology, Zhejiang 325000, China

* **Correspondence:** Email: ynsu@njzq.com.cn; raofeng2002@163.com.

Abstract: This paper characterizes the systemic dynamics of risk contagion within interconnected supply chain ecosystems by developing a degree-resolved susceptible-exposed-Infectious-recovered-susceptible (SEIRS) framework on heterogeneous network topologies. Utilizing the heterogeneous mean-field theory, we analytically derived a spectral threshold, the basic reproduction number $\mathcal{R}_0$, which governs the phase transition of risk cascades. We established that $\mathcal{R}_0 = 1$ constitutes a transcritical bifurcation point: the network resides in a distress-free state when $\mathcal{R}_0 < 1$, whereas a unique, globally attractive endemic equilibrium emerges when $\mathcal{R}_0 > 1$, signifying the onset of chronic systemic fragility. Sensitivity analysis revealed that the risk threshold is predominantly driven by the contagion intensity across business ties and the duration of latent vulnerability, while metabolic clearing mechanisms, such as firm exit and market attrition, effectively truncate the infectious window. Furthermore, we formulated an optimal control problem to identify targeted intervention strategies that minimize the aggregate social cost of disruptions against fiscal constraints. Numerical simulations on scale-free topologies demonstrated that targeted recovery stimulus effectively fosters a V-shaped resilience rebound, starving the contagion of susceptible hosts. Our results provide a theoretical foundation for re-engineering supply chain resilience and designing cost-effective regulatory stabilizers in the presence of network externalities.

Keywords: systemic risk contagion; heterogeneous mean-field theory; basic reproduction number; global stability analysis; optimal control theory
Mathematics Subject Classification: 90B15, 90B50

1. Introduction

The modern supply chain landscape is defined by a fundamental tension between operational efficiency and systemic fragility. While globalization and digital integration have fostered highly specialized and interconnected networks, they have simultaneously amplified the susceptibility of these systems to cascading disruptions [1,2]. In this hyper-connected environment, localized stochastic shocks, such as pandemic-induced labor shortages, widespread production shutdowns, supply disruptions, and geopolitical trade volatility, no longer remain isolated. Instead, they spread rapidly through counterparty exposures [3–5], often triggering nonlinear, large-scale functional failures in the global supply chain network [6, 7]. Such systemic risk cascades can destabilize entire industrial ecosystems, resulting in profound and prolonged socioeconomic consequences [8].

Effective supply chain risk governance is increasingly challenged by the structural complexity and inherent opacity of contemporary networked systems. Real-world supply chain ecosystems are typical nonlinear complex networks with prominent topological heterogeneity, rather than simplified homogeneous linear chains. Different enterprises hold distinct market positions, business scales, and cooperative scales, leading to obvious disparities in the number of upstream and downstream partnerships. This structural heterogeneity can be quantitatively described by the node degree distribution $P(k)$, which measures the probability that a randomly selected enterprise node maintains k business connection edges in the network.

Further, most modern supply chain systems present typical scale-free topological characteristics, whose degree distribution follows a classic power-law function:

$$P(k) \sim k^{-\gamma}, \quad \gamma > 2.$$

In such topological structures, a small number of core leading enterprises possess ultra-high node degrees and act as critical hubs for material flow, capital flow, and information transmission, while the vast majority of small and medium-sized peripheral enterprises only maintain limited and sparse cooperative relationships. Driven by this unbalanced node distribution, the overall high network connectivity constructed by dense transaction links greatly reduces the barriers of risk diffusion. The global connection compactness of supply chains can be further quantified by the algebraic connectivity derived from the Laplacian matrix eigenvalue, where higher connectivity accelerates the cross-node spillover and secondary diffusion of fragile shocks.

Enterprises exhibit heterogeneous resilience and anti-risk capabilities, and potential risk sources have become increasingly diversified and concealed in complex network environments [9, 10]. Conventional risk management frameworks, which predominantly rely on static evaluation and localized independent assessment [11, 12], are inherently inadequate for capturing the dynamic evolution and long-range contagion of risks across interconnected network nodes. Traditional epidemic models established under the homogeneous mixing assumption also fail to characterize the asymmetric transmission difference between core enterprises and marginal organizations.

To address these challenges, contemporary research has pivoted toward the synthesis of complex network theory and compartmental epidemiological modeling. One primary research stream leverages network science to characterize the topological determinants of risk diffusion [13]. Studies have demonstrated that supply chain architectures often exhibit small-world and scale-free properties, where the existence of high-degree hubs significantly lowers the threshold for systemic contagion [14–16].

Key topological parameters, such as the average degree and clustering coefficient, have been identified as critical drivers of both the speed and magnitude of risk cascades [17–19]. For instance, using computational modeling and network analysis, [16] revealed that global supply network structure drives risk diffusion and supply chain health, while also underscoring the critical role of supply network visibility. The authors applied stochastic CVaR (conditional value at risk) optimization to establish risk-averse viability boundaries in supply chains under disruption propagation, revealing that larger viability spaces enhance both worst-case and average resilience [19].

A parallel research stream employs epidemiological frameworks, such as SIS, SIR, and SIRS models, to simulate the temporal evolution of risk spreading [20–22]. These compartmental approaches have been adapted to supply chain contexts to determine the basic reproduction number ($\mathcal{R}_0$), a critical threshold governing the transition between risk extinction and endemic persistence [23–25]. Recent work has shown that the stability of supply networks is highly sensitive to infection rates and the immunity or recovery capacity of individual firms, underscoring the necessity of data-driven surveillance and early-stage regulatory intervention [26–30]. For example, an improved SIRS model based on the actual elimination of node-type companies was established to analyze risk transmission mechanisms and the influence of key parameters on risk propagation and node behavior within multi-driver supply chain networks [26]. Chang et al. [29] employed an SEIRS epidemic model to dynamically simulate risk contagion paths in green supply chain finance, identifying the risk contagion rate as the key determinant of enterprise bankruptcy and the repeated infection rate as the critical factor weakening supply chain recovery. In [30], the authors developed a government-intervened risk propagation model for complex supply chain networks under public emergencies using an enhanced SEIR framework, demonstrating that controlling the basic reproduction number $\mathcal{R}_0$ enables effective risk containment.

Despite these advancements, critical research gaps remain. Most existing models utilize simplified dynamics that overlook two essential physical realities: (i) the manifestation lag, or the latent period during which an enterprise has absorbed a shock but has not yet defaulted; and (ii) resilience erosion, representing the temporal decay of recovered firms' immunity. Furthermore, while the role of external assistance is acknowledged, there is a lack of rigorous optimal control frameworks derived from higher-order systems like the SEIRS model. Our research fills these voids by developing a unified SEIRS-based analytical framework that incorporates both latent states and waning resilience, while simultaneously deriving optimal government intervention strategies to minimize aggregate social costs under fiscal constraints.

This paper characterizes the systemic dynamics of risk contagion and regulatory stabilization within complex supply chain networks. By mapping the lifecycle of operational disruptions onto a degree-resolved SEIRS framework, we elucidate how localized shocks evolve into network-wide cascades. The contributions of this study are threefold:

1. We develop an SEIRS framework that explicitly captures two critical physiological traits of supply chain distress: the latent-risk phase (E), representing firms that have absorbed a shock but have not yet manifested operational failure, and the temporal decay of resilience ($R \to S$), reflecting the finite nature of restructuring immunity and the return to vulnerability.
2. Utilizing heterogeneous mean-field theory, we derive the spectral threshold, the basic reproduction number $\mathcal{R}_0$, which governs the phase transition between risk extinction and endemic persistence. Our analysis identifies how network topology interacts with contagion parameters to define the system's global stability.

3. We formulate a regulatory intervention problem using optimal control theory. By treating the public recovery stimulus as a targeted instrument, we identify the optimal stimulus threshold that minimizes the network-wide social cost, ensuring that risk suppression is achieved without incurring disproportionate fiscal overstretch due to diminishing marginal returns.

The remainder of this paper is structured as follows. Section 2 formulates the degree-resolved SEIRS dynamics and establishes the fundamental well-posedness of the system. Section 3 provides a stability analysis of the distress-free and endemic equilibria using Lyapunov functionals and LaSalle's invariance principle. Section 4 introduces the optimal control framework, proves the existence of an optimal policy, and characterizes its structure via Pontryagin's minimum principle. Section 5 presents numerical simulations on scale-free topologies to quantify the sensitivity of risk cascades to structural parameters and intervention intensities. Finally, Section 6 concludes with a synthesis of managerial insights and policy recommendations.

2. Model formulation and preliminary analysis

We consider a supply chain network consisting of N nodal enterprises, whose interdependencies are formalized through a complex topological structure. To capture the multi-stage evolution of systemic distress, we categorize each enterprise into one of four mutually exclusive states, mapping the SEIRS compartmental framework onto the operational life cycle of risk (see Figure 1):

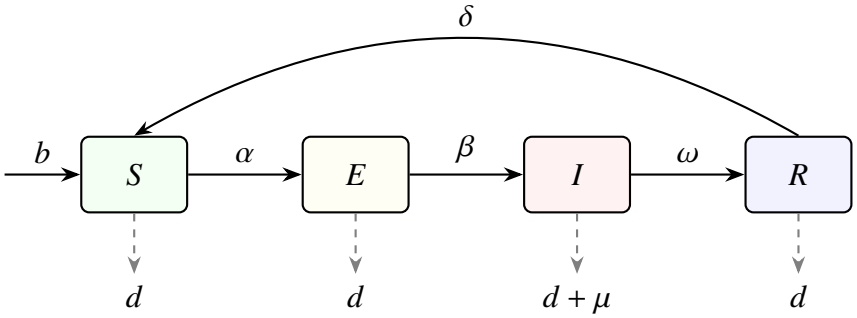

Figure 1. Mechanistic flow and state transition logic of the supply chain SEIRS system.

1. Resilient (S): Healthy enterprises operating at nominal capacity, possessing the full potential to absorb or propagate shocks.
2. Latent (E): Enterprises that have absorbed a hidden operational shock. In this stage, the firm carries a latent vulnerability. While deliveries remain superficially on time, internal stability is compromised, and the firm acts as a silent carrier of systemic pressure. In real-world supply chain data, the latent state can be proxied using early warning indicators such as payment delays (e.g., accounts payable days extending beyond contractual terms), operational degradation (e.g., declining on-time delivery rates), or financial distress signals (e.g., credit rating downgrades). These observable metrics precede formal default or bankruptcy, which corresponds to the infectious state. Transition rates between states can then be estimated empirically by tracking cohorts of firms over time.
3. Distressed (I): Enterprises are in a state of active disruption. Here, the risk has manifested into operational failure, triggering cascading delays and order cancellations across downstream business ties.

4. Restructured (R): Enterprises that have successfully mitigated the disruption through restorative interventions (e.g., dual-sourcing or liquidity injections). These firms possess temporary structural immunity, though this protection is finite and subject to erosion.

The dynamical transition between these states reflects the underlying physics of risk contagion. A resilient enterprise (S) transitions to the latent state (E) at a contagion intensity α, governed by its counterparty exposure. The latent threat then activates into a full-scale disruption (I) at a manifestation rate β, representing the time-lag between shock absorption and functional breakdown. Subsequently, distressed nodes are restored to the restructured state (R) at a recovery rate ω, reflecting the system's endogenous and exogenous restorative capacity. Finally, as post-crisis buffers deplete or contingency contracts expire, restructured firms revert to the susceptible state (S) at a resilience decay rate δ, completing the cycle of systemic vulnerability.

To ensure the analytical tractability and managerial relevance of the risk contagion mechanism, we establish the following formal hypotheses, grounding the SEIRS framework in the physical realities of supply chain interdependencies.

(A1) **Network topology:** Supply chain networks are characterized by continuous flux, where firms enter or exit based on strategic optimization and market attrition [1]. To isolate the infectious dynamics from structural drift, we assume an instantaneous replacement mechanism [13, 31, 32]. Specifically, any enterprise with degree k that is removed from the market, either through natural attrition (d) or risk-induced insolvency (μ), is immediately replaced by a new entrant in the susceptible state (S_k) with identical connectivity. This ensures $\mathrm{d}N_k/\mathrm{d}t = 0$, maintaining a constant degree distribution P_k and a stationary total population N throughout the evolutionary process. This instantaneous replacement assumption is imposed only to stabilize the network topological structure and eliminate the interference of long-term structural drift on risk contagion dynamics. Therefore, it is applicable exclusively to short - through medium-term systemic risk contagion assessment.

(A2) **Inter-firm coupling:** Risk contagion is strictly contingent upon bilateral counterparty exposure [5]. Enterprises are assumed to be independent in the absence of transactional or contractual linkages. Within the supply chain architecture, this coupling reflects the physical physics of inter-firm dependencies: financial distress and operational shocks propagate through both credit linkages (upstream flow of default risk) and logistical linkages (downstream flow of disruption), justifying an undirected graph representation for holistic cascade analysis [10].

(A3) **Latent risk lag effect:** The system explicitly captures the manifestation lag of disruptions [33]. An enterprise may absorb a systemic shock and enter a latent-risk state (E), maintaining superficial delivery continuity while carrying hidden internal instability. Furthermore, the immunity acquired through restorative measures (R), such as restructuring or liquidity injections, is assumed to be finite. The temporal decay of this resilience (δ) reflects the depletion of crisis buffers, after which firms revert to a susceptible state (S) [34].

(A4) **Risk mitigation intervention:** To mitigate systemic collapses, we assume an exogenous regulatory body deploys targeted intervention instruments [35, 36]. This mirrors the public policy framework for managing systemic risks, where interventions augment the network's endogenous restorative capacity [37]. Such measures include fiscal subsidies or policy-driven immunization for systemically important hubs, aimed at truncating the contagion window.

Nodal enterprises are categorized according to their degree k, signifying their connectivity or number of direct trading partners, in order to capture the stochastic nature of risk evolution within a complex supply chain topology. Defining $S_k(t), E_k(t), I_k(t)$, and $R_k(t)$ as the densities of susceptible, exposed, infected, and recovered firms within each degree class, this framework enables a granular tracking of risk dynamics. The total population $N_k(t)$ for kth-degree enterprises is governed by the conservation identity $S_k(t) + E_k(t) + I_k(t) + R_k(t) = N_k(t)$.

By synthesizing risk contagion mechanisms characteristic of complex networks [9, 10] with the heterogeneous mean-field theory [31, 38–40], we characterize the contagion dynamics through the following SEIRS compartmental system:

$$\begin{cases} \dfrac{\mathrm{d}S_k(t)}{\mathrm{d}t} = b - \alpha k S_k(t)\Theta(t) + \delta R_k(t) - dS_k(t), \\ \dfrac{\mathrm{d}E_k(t)}{\mathrm{d}t} = \alpha k S_k(t)\Theta(t) - (\beta + d)E_k(t), \\ \dfrac{\mathrm{d}I_k(t)}{\mathrm{d}t} = \beta E_k(t) - (\omega + d + \mu)I_k(t), \\ \dfrac{\mathrm{d}R_k(t)}{\mathrm{d}t} = \omega I_k(t) - (\delta + d)R_k(t), \end{cases} \tag{2.1}$$

where the dynamic interaction is mediated by $\Theta(t)$, defined as the probability that a susceptible enterprise is linked to a distressed (risky) counterpart. Following the connectivity-weighted transmission logic [41], the contagion pressure is formulated as

$$\Theta(t) = \frac{1}{\langle k \rangle} \sum_{k=1}^{n} k P_k \frac{I_k(t)}{N_k(t)}, \quad \text{with} \quad \langle k \rangle = \sum_{k=1}^{n} k P_k, \tag{2.2}$$

where P_k represents the degree distribution, characterizing the topological architecture of the supply chain. $\langle k \rangle$ denotes the average connectivity of the network. The parameters $b, \alpha, \beta, \omega, \delta, d, \mu$ signify the entry rate, infection (contagion) rate, transition rate to the clinical state, recovery rate, immunity loss rate, exit (attrition) rate, and risk-induced failure rate, respectively. The evolutionary system (2.1) is subject to the following bounded initial conditions:

$$\begin{aligned} &0 \le S_k(0), E_k(0), I_k(0), R_k(0) \le \frac{b}{d}, \\ &S_k(0) + E_k(0) + I_k(0) + R_k(0) = N_k(0), \quad \forall k \in \{1, 2, \ldots, n\}, \end{aligned} \tag{2.3}$$

and its parameters are summarized in Table 1.

Table 1. Parameters of the SEIRS system (2.1).

Parameter	Description
b	The entry number of new enterprises
α	The risk infection rate of healthy enterprises
β	The conversion rate of risk latent enterprises to risk infectious enterprises
ω	The risk management capability of enterprises
d	Existing enterprise exit rate
μ	Market elimination rate
δ	The risk immunization loss rate

Having defined the degree-dependent SEIRS dynamics and the mean-field coupling term $\Theta(t)$, we now establish a fundamental property of system (2.1): the positivity of $\Theta(t)$ ensures that all degree classes remain dynamically coupled, preventing the system from decomposing into independent subsystems. This irreducibility property is formalized in the following lemma 2.1.

Lemma 2.1. *For the SEIRS system* (2.1) *with* $\Theta(t) = \frac{1}{\langle k\rangle}\sum_k kP_k\frac{I_k(t)}{N_k(t)}$*, the following holds: If there exists any degree class with* $I_{k_0}(0) > 0$ *and* $S_k(0) > 0$ *for all* k*, then* $\Theta(t) > 0$ *for all* $t > 0$*. Consequently, all degree classes are dynamically coupled through* $\Theta(t)$*, and the system is irreducible.*

Proof. Since $kP_k/\langle k\rangle > 0$ for all k with $P_k > 0$, $\Theta(t) > 0$ iff $\exists k : I_k(t) > 0$. Given $I_{k_0}(0) > 0$, continuity implies $I_{k_0}(t) > 0$ for small t. For any other degree class k, the term $\alpha k S_k(t)\Theta(t)$ in $\frac{\mathrm{d}S_k}{\mathrm{d}t}$ is strictly positive because $S_k(0) > 0$ and $\Theta(t) > 0$. Thus, susceptible enterprises in class k become exposed, making the dynamics of all degree classes interdependent. Hence, the system cannot be decomposed into independent subsystems. □

To ensure the dynamical system (2.1) is a rigorous representation of supply chain risk evolution, we first establish the boundedness and non-negativity of its trajectories.

Lemma 2.2. *Let* $(S_k(t), E_k(t), I_k(t), R_k(t))$ *be a trajectory of system* (2.1) *originating from the initial conditions* (2.3)*. Then, the feasible region defined by*

$$\Omega = \Big\{(S_1, E_1, I_1, R_1, \ldots, S_n, E_n, I_n, R_n) \in \mathbb{R}_+^{4n} : \\ S_k(t) + E_k(t) + I_k(t) + R_k(t) \le \frac{b}{d}, \quad \forall k \in \{1, \ldots, n\}\Big\} \tag{2.4}$$

is positively invariant with respect to (2.1)*.*

Remark 1. *Lemma 2.2 ensures that the enterprise population within each degree class remains economically meaningful, specifically, non-negative and uniformly bounded, throughout the temporal evolution of the system. This result provides the requisite mathematical foundation for subsequent stability analysis and ensures that the system accurately reflects the finite capacity and structural constraints of the firm-to-firm network under financial distress. The detailed proof is provided in the Appendix.*

The stationary states of the dynamical system (2.1) are obtained by setting the time derivatives to zero, yielding the following algebraic system:

$$\begin{cases} 0 = b - \alpha k S_k \Theta - \delta R_k - d S_k, \\ 0 = \alpha k S_k \Theta - (\beta + d) E_k, \\ 0 = \beta E_k - (\omega + d + \mu) I_k, \\ 0 = \omega I_k - (\delta + d) R_k. \end{cases} \tag{2.5}$$

In the absence of systemic distress, the system admits a unique distress-free equilibrium (DFE), denoted by $\mathbf{E}^0$, where $E_k = I_k = R_k = 0$ for all $k \in \{1, \ldots, n\}$. Consequently, $S_k^0 = b/d$, and the DFE is characterized as

$$\mathbf{E}^0 = \left(\underbrace{\frac{b}{d}, 0, 0, 0}_{\text{degree } 1}, \ldots, \underbrace{\frac{b}{d}, 0, 0, 0}_{\text{degree } n} \right) \in \mathbb{R}_+^{4n}.$$

To determine the threshold for risk persistence, we employ the next-generation matrix formalism [42,43]. Let $x_k = (E_k, I_k)^{\mathrm{T}}$ represent the distressed (infected) compartments of degree-k nodes. The linearized distress dynamics can be decomposed as

$$\frac{\mathrm{d}x_k}{\mathrm{d}t} = \mathcal{F}_k(x) - \mathcal{V}_k(x), \quad k = 1, 2, \ldots, n,$$

where the rate of new risk appearances $\mathcal{F}_k(x)$ and the rate of compartmental transitions $\mathcal{V}_k(x)$ are given by

$$\mathcal{F}_k(x) = \begin{bmatrix} \alpha k S_k \Theta \\ 0 \end{bmatrix}, \quad \mathcal{V}_k(x) = \begin{bmatrix} (\beta + d) E_k \\ -\beta E_k + (\omega + d + \mu) I_k \end{bmatrix}. \tag{2.6}$$

Note that $\mathcal{F}_k(x)$ represents the rate at which risk propagates to susceptible suppliers, effectively transferring firms into the exposed compartment. $\mathcal{V}_k(x)$ characterizes the internal transfer between distressed states and the exit from the distressed pool due to recovery, attrition, or risk-induced bankruptcy.

Let $\mathscr{M}$ and $\mathscr{N}$ denote the Jacobian matrices of $\mathcal{F} = (\mathcal{F}_1, \ldots, \mathcal{F}_n)^{\mathrm{T}}$ and $\mathcal{V} = (\mathcal{V}_1, \ldots, \mathcal{V}_n)^{\mathrm{T}}$ evaluated at $\mathbf{E}^0$, respectively. Then,

$$\mathscr{M} = \left(\mathcal{P}_{kj} \right)_{2n \times 2n}, \quad \mathscr{N} = \operatorname{diag} \left(\mathcal{Q}_1, \ldots, \mathcal{Q}_n \right)_{2n \times 2n},$$

where the block entries are derived as

$$\mathcal{P}_{kj} = \begin{bmatrix} 0 & \dfrac{k j \alpha P_j}{\langle k \rangle} \\ 0 & 0 \end{bmatrix}, \quad \mathcal{Q}_k = \begin{bmatrix} \beta + d & 0 \\ -\beta & \omega + d + \mu \end{bmatrix}.$$

Here, $\mathscr{M}$ represents the transmission dynamics across different degree classes, while $\mathscr{N}$ accounts for the individual transition and failure rates.

In the context of supply chain networks, the basic reproduction number $\mathcal{R}_0$ serves as a threshold parameter for systemic risk. It quantifies the average number of secondary disruptions generated by a

single distressed firm introduced into a fully resilient network. Following the next-generation approach, $\mathcal{R}_0$ is defined as the spectral radius of the next-generation matrix $\mathscr{M}\mathscr{N}^{-1}$:

$$\mathcal{R}_0 = \rho\left(\mathscr{M}\mathscr{N}^{-1}\right).$$

Through direct algebraic derivation, we obtain

$$\mathcal{R}_0 = \frac{\langle k^2\rangle\alpha\beta}{\langle k\rangle(\beta + d)(\omega + d + \mu)}, \tag{2.7}$$

where $\langle k^2\rangle = \sum_{k=1}^{n} k^2 P_k$. In this formulation, the ratio $\langle k^2\rangle/\langle k\rangle$ captures the impact of network heterogeneity on risk diffusion. This ratio acts as a network heterogeneity amplifier, implying that a small number of high-degree hub enterprises, if disrupted, disproportionately amplify systemic risk cascades across the entire supply chain ecosystem. The term α reflects the contagion intensity, β is the latent transition rate, d denotes the exogenous attrition rate, and the denominator $(\omega + d + \mu)$ represents the cumulative rate of risk abatement and terminal failure.

We now establish the existence and uniqueness of the risk-endemic equilibrium (REE), denoted by $\mathbf{E}^+ = (S_k^+, E_k^+, I_k^+, R_k^+)$. The REE represents a steady state where risk persists within the supply chain network despite ongoing operational flows and restorative interventions. In this regime, the distribution of firms across the four states: resilient (S), latently disrupted (E), actively distressed (I), and restructured (R), settles into a persistent time-invariant proportion across each degree stratum.

By solving the algebraic system derived from setting the right-hand sides of (2.1) to zero, we characterize the components of the unique REE as follows:

$$\begin{aligned}
S_k^+ &= \frac{b(d+\delta)(d+\mu+\omega)(\beta+d)}{\mathcal{D}_k},\\
E_k^+ &= \frac{b\alpha\Theta k(d+\delta)(d+\mu+\omega)}{\mathcal{D}_k},\\
I_k^+ &= \frac{b\alpha\Theta k\beta(d+\delta)}{\mathcal{D}_k},\\
R_k^+ &= \frac{b\alpha\Theta k\beta\omega}{\mathcal{D}_k},
\end{aligned} \tag{2.8}$$

where the common denominator $\mathcal{D}_k$ is defined as

$$\mathcal{D}_k := (d + \alpha\Theta k)(d+\delta)(d+\mu+\omega)(\beta+d) + d\omega\big[(d+\delta)(\beta+d) + \alpha\Theta k(\beta+d+\delta)\big].$$

The strict positivity of $\mathcal{D}_k$ for all feasible parameter sets ensures that $\mathbf{E}^+ \in \mathbb{R}_+^{4n}$ whenever the risk-contagion pressure $\Theta > 0$, confirming the biological and economic feasibility of the endemic state.

Theorem 2.3. *The supply chain risk contagion system* (2.1) *admits a unique and globally attractive risk-endemic equilibrium* $\mathbf{E}^+$ *if and only if the basic reproduction number* $\mathcal{R}_0 > 1$. *If* $\mathcal{R}_0 \le 1$, *the distress-free equilibrium* $\mathbf{E}^0$ *is the only steady state within the feasible region* Ω.

For convenience, a detailed proof of Theorem 2.3 is presented in the Appendix.

Remark 2. *Theorem 2.3 provides a critical threshold for supply chain resilience. When $\mathcal{R}_0 > 1$, any localized disruption, such as a regional logistics failure or a Tier-N supplier insolvency, is no longer transient but sparks a self-sustaining contagion. In this endemic regime, the network remains in a state of chronic distress, where each disrupted firm, on average, compromises more than one downstream partner before recovering.*

The equilibrium shares $(S_k^+, E_k^+, I_k^+, R_k^+)$ form a strategic early-warning dashboard for supply chain managers. A persistently high proportion of exposed (E_k^+) and infected (I_k^+) nodes signals systemic output loss and chronic lead-time inflation, even without new disruptions. Because the contagion pressure scales with node degree k, managers must prioritize interventions at high-degree hubs, such as critical orchestrators or sole-source suppliers, to maximize resilience. Effective mitigation aims to drive the effective reproduction number $\mathcal{R}_0$ below 1 through three levers: diversification (reducing α) via multi-sourcing; agility (increasing ω) through pre-positioned capacity or accelerated recovery; and buffer management by improving visibility to contain latent risks ($E \to I$) before they escalate into active disruptions.

3. Stability of the steady state

To establish a rigorous foundation for the stability of the distress-free equilibrium $\mathbf{E}^0$ and the risk-endemic equilibrium $\mathbf{E}^+$, we first delineate the structural properties of the dynamic system. These properties ensure that the system is biologically and economically well-posed.

Let the state space be $\Omega \subset \mathbb{R}_+^{4n}$. We define the state vector as $\mathbf{x} = (\mathbf{x}_S, \mathbf{x}_E, \mathbf{x}_I, \mathbf{x}_R)^\mathsf{T}$, where each $\mathbf{x}_i$ represents the density within compartment $i \in \{S, E, I, R\}$. The distress-free manifold $\mathbb{X}$ is defined as the set of states where no operational disruption exists:

$$\mathbb{X} = \{\mathbf{x} \in \Omega \mid \mathbf{x}_E = \mathbf{0}, \mathbf{x}_I = \mathbf{0}\}. \tag{3.1}$$

Consistent with the next-generation matrix framework, the following structural conditions are satisfied:

(C1) The functions $\mathcal{F}_i$, $\mathcal{V}_i^-$, and $\mathcal{V}_i^+$ are non-negative for all $\mathbf{x} \geq \mathbf{0}$. This ensures that the non-negative orthant $\mathbb{R}_+^{4n}$ is positively invariant, meaning enterprise populations never become negative.

(C2) If a degree class lacks exposed or infected firms ($\mathbf{x}_{E,I} = \mathbf{0}$), the outward transfer from these compartments vanishes ($\mathcal{V}_{E,I}^- = \mathbf{0}$), implying that firms cannot exit a distressed state that is not yet populated.

(C3) For the resilient and recovered compartments ($i \in \{S, R\}$), $\mathcal{F}_i = \mathbf{0}$. This assumes that new infections only enter the system through the exposed compartment, excluding spontaneous risk generation without a contagion source.

(C4) If the system resides on the distress-free manifold ($\mathbf{x} \in \mathbb{X}$), then $\mathcal{F}_{E,I}(\mathbf{x}) = \mathbf{0}$ and $\mathcal{V}_{E,I}^+(\mathbf{x}) = \mathbf{0}$. This guarantees that a supply chain network free of latent or active disruptions will remain resilient unless an external shock introduces risk.

(C5) Let $\mathcal{N}$ be the Jacobian of the transition dynamics. In the absence of new risk arrivals ($\mathcal{F}_{E,I} = \mathbf{0}$), the system $\dot{x} = -\mathcal{V}(x)$ is globally asymptotically stable at the origin. This implies that the internal clearing mechanisms (recovery and exit) are sufficient to dissipate existing distress if no further contagion occurs.

The threshold behavior of the system at the distress-free equilibrium is characterized by the following theorem.

Theorem 3.1 (Local stability of the DFE)**.** *Under conditions (C1)–(C5), the distress-free equilibrium* $\mathbf{E}^0$ *is locally asymptotically stable if* $\mathcal{R}_0 < 1$*, and unstable if* $\mathcal{R}_0 > 1$.

The proof of Theorem 3.1 can be found in the Appendix.

Remark 3. *The condition* $\mathcal{R}_0 < 1$ *represents a resiliency threshold. In this regime, each distressed firm, on average, compromises fewer than one downstream partner before it either recovers or exits the network. Consequently, sporadic disruptions remain localized and eventually dissipate, allowing the network to self-heal and return to a fully operational state. However, once* $\mathcal{R}_0$ *crosses unity, a bifurcation occurs. The same localized shock now acts as a seed for a systemic cascade. Because each infected node passes the risk to more than one neighbor, the disruption amplifies through counterparty exposures. In this scenario, the distress-free state becomes an unstable repeller, and the system inevitably settles into an endemic state of chronic instability. Managers must therefore treat* $\mathcal{R}_0$ *as a systemic risk KPI (key performance indicator), where interventions should aim at decoupling connectivity or accelerating recovery to pull* $\mathcal{R}_0$ *back below the unit threshold.*

The local stability analysis ensures resilience against infinitesimal shocks. However, from a systemic risk perspective, it is imperative to determine whether the network can recover from large-scale, heterogeneous disruptions. The following theorem establishes the global threshold property of the system.

Theorem 3.2 (Global asymptotic stability of the DFE)**.** *The distress-free equilibrium* $\mathbf{E}^0$ *of the supply chain risk contagion system* (2.1) *is globally asymptotically stable in the feasible region* Ω *if and only if* $\mathcal{R}_0 \le 1$.

Proof. We construct a composite Lyapunov functional $V : \Omega \to \mathbb{R}_+$ to establish the global attractiveness of $\mathbf{E}^0$. Let $S_k^0 = b/d$ denote the saturation level of resilient firms in each degree class. Inspired by the Volterra-type entropy structures used in epidemic dynamics [38], we define

$$V(t) = \sum_{k=1}^{n} \frac{kP_k}{\langle k \rangle} \left[S_k^0 \Phi\left(\frac{S_k}{S_k^0}\right) + E_k + \frac{\beta + d}{\beta} I_k \right], \tag{3.2}$$

where $\Phi(x) = x - 1 - \ln x$ is a strictly convex, positive-definite function for $x > 0$, vanishing only at $x = 1$. Consequently, $V(\mathbf{x}) \ge 0$ on Ω, and $V(\mathbf{x}) = 0$ if and only if $\mathbf{x} = \mathbf{E}^0$.

Differentiating V along the trajectories of (2.1), we analyze the time evolution of the resilient and distressed components. For the resilient component V_S, using $b = dS_k^0$, we obtain

$$\begin{aligned} \dot{V}_S &= \sum_{k=1}^{n} \frac{kP_k}{\langle k \rangle} \left(1 - \frac{S_k^0}{S_k}\right) \left(d(S_k^0 - S_k) - \alpha k S_k \Theta + \delta R_k \right) \\ &= \sum_{k=1}^{n} \frac{kP_k}{\langle k \rangle} \left[-\frac{d(S_k - S_k^0)^2}{S_k} - \alpha k (S_k - S_k^0)\Theta + \delta R_k \left(1 - \frac{S_k^0}{S_k}\right) \right]. \end{aligned} \tag{3.3}$$

Combining $\dot{V}_S$ with the derivatives of the exposed and infected components, $\dot{V}_E$ and $\dot{V}_I$, the aggregate orbital derivative $\dot{V}$ satisfies

$$\dot{V} \le \sum_{k=1}^{n} \frac{kP_k}{\langle k \rangle} \left[-\frac{d(S_k - S_k^0)^2}{S_k} + \alpha k S_k^0 \Theta - \frac{(\beta + d)(\omega + d + \mu)}{\beta} I_k \right]$$

$$= -\sum_{k=1}^{n} \frac{kP_k d(S_k - S_k^0)^2}{\langle k\rangle S_k} + \alpha \frac{b}{d} \underbrace{\left(\frac{1}{\langle k\rangle} \sum_{k=1}^{n} k^2 P_k \frac{I_k}{N_k} \right)}_{\Theta\cdot\langle k\rangle} - \frac{(\beta + d)(\omega + d + \mu)}{\beta} \sum_{k=1}^{n} \frac{kP_k}{\langle k\rangle} I_k. \tag{3.4}$$

Utilizing the definition of $\mathcal{R}_0$ and the fact that $N_k \le S_k^0$ in the steady state, we can upper-bound the interaction term. After factoring out the common distress intensities, we arrive at

$$\dot{V} \le -\sum_{k=1}^{n} \frac{kP_k d(S_k - S_k^0)^2}{\langle k\rangle S_k} + \frac{(\beta + d)(\omega + d + \mu)}{\beta\langle k\rangle} (\mathcal{R}_0 - 1) \sum_{k=1}^{n} kP_k I_k. \tag{3.5}$$

If $\mathcal{R}_0 \le 1$, then $\dot{V} \le 0$ for all $\mathbf{x} \in \Omega$. Specifically, $\dot{V} = 0$ implies $S_k = S_k^0$ and $(\mathcal{R}_0 - 1)I_k = 0$. In the invariant set where $\dot{V} = 0$, it follows from the system equations that E_k, I_k, R_k must all vanish. According to LaSalle's invariance principle, every trajectory in Ω converges asymptotically to the largest invariant subset where $\dot{V} = 0$, which is the singleton $\{\mathbf{E}^0\}$. Thus, the distress-free equilibrium is globally asymptotically stable. □

Remark 4. *Theorem 3.2 provides a profound guarantee for systemic operational continuity. While local stability only ensures recovery from minor perturbations, global stability under $\mathcal{R}_0 < 1$ implies that the supply chain possesses a topological self-healing capability. Regardless of the magnitude of the initial shock, whether it is a catastrophic black swan event or a targeted failure of high-degree hubs, the network will inherently dissipate the distress over time. From a managerial standpoint, the threshold condition $\mathcal{R}_0 = 1$ translates into a hard policy constraint, requiring a system-wide rather than firm-level perspective. Managers must actively tune key operational parameters to ensure $\mathcal{R}_0 < 1$, thereby containing risk contagion and enabling long-term network robustness. Concrete interventions include: (1) accelerating recovery velocity by shortening the latent period (β^{-1}) and expediting restructuring (ω), effectively draining contagion pressure; (2) reducing structural coupling (α) through dual-sourcing or regionalization to weaken transmission across business ties; and (3) maintaining a healthy rate of firm entry and exit (d, b) to sustain network metabolism and prevent stagnation of distressed assets. Collectively, these measures shift the network from transient survival to durable equilibrium resilience.*

When the basic reproduction number $\mathcal{R}_0$ exceeds unity, the system undergoes a bifurcation, where the distress-free equilibrium loses its stability and a unique positive equilibrium emerges. The following analysis establishes that this endemic state is a global attractor, implying the inevitable convergence of the network toward a chronic state of risk.

We first present a pivotal result from the theory of sub-homogeneous systems, which serves as our primary analytical tool.

Lemma 3.3. *Consider an autonomous system $\dot{x} = g(x)$ defined on $\mathbb{R}^n_+$, where g is a C^1 function such that:*

(H1) The origin is an equilibrium ($g(0) = 0$), the orthant $\mathbb{R}^n_+$ is forward invariant, and g is dissipative (maps bounded sets into bounded sets).

(H2) The Jacobian $\mathsf{D}g(x)$ is irreducible for every $x \in \mathbb{R}^n_+$, reflecting strong connectivity in the underlying system structure.

(H3) g is strictly sub-homogeneous: $g(\varepsilon x) > \varepsilon g(x)$ for all $\varepsilon \in (0, 1)$ and $x \gg 0$.

Under these conditions, if the spectral abscissa $s(\mathsf{D}g(0)) > 0$, the system possesses a unique non-trivial equilibrium $x^+ \gg 0$ that is globally asymptotically stable in $\mathbb{R}^n_+ \setminus \{0\}$.

Remark 5. *Lemma 3.3 provides a powerful analytical framework for establishing the existence, uniqueness, and global stability of non-trivial equilibria in networked systems with positive feedback. Condition (H2) (irreducibility of the Jacobian) ensures that system* (2.1) *cannot decompose into independent subsystems, which in our supply chain network is guaranteed by the positivity of $\Theta(t)$ established in Lemma 2.1. Condition (H3) (strict sub-homogeneity) captures the diminishing returns characteristic of epidemic-type propagation: doubling the scale of infection less than doubles the rate of new infections, a property that holds for our SEIRS dynamics due to the saturation effect in the transmission term $\alpha k S_k \Theta$. The condition $s(\mathsf{D}g(0)) > 0$ is precisely equivalent to $\mathcal{R}_0 > 1$ in our system, as the spectral abscissa of the Jacobian at the disease-free equilibrium determines the initial growth rate of perturbations. Consequently, Lemma 3.3 allows us to conclude that when $\mathcal{R}_0 > 1$, the system converges to a unique globally attractive endemic equilibrium, ruling out the possibility of multiple steady states or sustained oscillations.*

Theorem 3.4 (Global stability of the REE)**.** *If $\mathcal{R}_0 > 1$, the unique risk-endemic equilibrium $\mathbf{E}^+$ of the supply chain system* (2.1) *is globally asymptotically stable in $\Omega \setminus \mathbb{X}$.*

Proof. By the invariance properties established in Theorem 2.2, we restrict our analysis to the compact simplex Ω. As $t \to \infty$, the conservation law $N_k(t) \to b/d$ allows us to reduce the dimensionality of the system. By substituting $S_k = b/d - E_k - I_k - R_k$, we focus on the limiting auxiliary system for the distressed compartments (E_k, I_k, R_k):

$$\begin{cases} \dot{E}_k = \alpha k \left(\dfrac{b}{d} - E_k - I_k - R_k \right) \Theta - (\beta + d) E_k, \\ \dot{I}_k = \beta E_k - (\omega + d + \mu) I_k, \\ \dot{R}_k = \omega I_k - (\delta + d) R_k. \end{cases} \tag{3.6}$$

Let $\boldsymbol{g}(\boldsymbol{x})$ denote the vector field of (3.6). We verify the conditions of Lemma 3.3 as follows:

1. The non-negativity of the boundary flow and the boundedness of Ω satisfy (H1).

2. The Jacobian $\mathsf{D}\boldsymbol{g}(\boldsymbol{x})$ exhibits a block-structure where coupling between different degree classes k and j is mediated by the contagion pressure Θ. Since the supply chain network is assumed to be connected ($P_k > 0$ for $k \in \{1, \ldots, n\}$), any distressed node can potentially influence any other node through the mean-field Θ. This ensures that $\mathsf{D}\boldsymbol{g}(\boldsymbol{x})$ is irreducible for $x \gg 0$.

3. For any $\varepsilon \in (0, 1)$, we evaluate $g_{k,1}(\varepsilon \boldsymbol{x})$:

$$\begin{aligned} g_{k,1}(\varepsilon \boldsymbol{x}) &= \alpha k \left(\frac{b}{d} - \varepsilon (E_k + I_k + R_k) \right) \Theta(\varepsilon \boldsymbol{x}) - (\beta + d) \varepsilon E_k \\ &= \varepsilon \left[\alpha k \left(\frac{b}{\varepsilon d} - (E_k + I_k + R_k) \right) \Theta(\boldsymbol{x}) - (\beta + d) E_k \right]. \end{aligned}$$

Since $b/\varepsilon d > b/d$ for $\varepsilon < 1$, it follows that $g_{k,1}(\varepsilon \boldsymbol{x}) > \varepsilon g_{k,1}(\boldsymbol{x})$. The linearity of the other components in (3.6) ensures $g_{k,i}(\varepsilon \boldsymbol{x}) = \varepsilon g_{k,i}(\boldsymbol{x})$ for $i = 2, 3$. Thus, $\boldsymbol{g}$ is strictly sub-homogeneous.

4. The spectral abscissa $s(\mathsf{D}\boldsymbol{g}(0))$ coincides with the condition $\mathcal{R}_0 > 1$ derived via the next-generation matrix. By Lemma 3.3, the reduced system possesses a unique globally stable positive equilibrium. By

the theory of asymptotic autonomous systems, the full system (2.1) inherits this global stability, and every trajectory in $\Omega \setminus \mathbb{X}$ converges to $\mathbf{E}^+$. □

Remark 6. *Theorem 3.4 reveals a critical and somewhat alarming property of systemic risk: path-independence. Once the network's structural parameters (transmission rates, recovery speeds, and connectivity) dictate that $\mathcal{R}_0 > 1$, the system is predestined to reach the endemic state $\mathbf{E}^+$, regardless of the initial scale or location of the disruption.*

4. Optimal risk control

Governmental responses to systemic supply-chain disruptions are inherently complex, requiring multi-dimensional and multi-stage coordination to bolster network resilience and truncate risk cascades [44,45]. In a fiscally constrained environment, the central policy challenge lies in designing targeted, degree-resolved intervention strategies that minimize the operational footprint of disruptions while maintaining fiscal sustainability.

We formalize public assistance as a time-varying control vector $\boldsymbol{v}(t)$, integrated into the heterogeneous SEIRS framework (2.1). Let the admissible control space be defined by

$$\mathbb{V} = \{\boldsymbol{v} \in L^\infty(0, T; \mathbb{R}^n) \mid 0 \le v_k(t) \le 1, \text{ a.e. } t \in [0, T], \forall k \in \{1, \dots, n\}\},$$

where $v_k(t)$ represents the intensity of the recovery stimulus (e.g., liquidity injections, administrative fast-tracking, or logistical subsidies) directed toward distressed firms of degree k. The controlled dynamics are characterized by

$$\begin{cases} \dot{S}_k(t) = b - \alpha k S_k(t)\Theta(t) + \delta R_k(t) - d S_k(t), \\ \dot{E}_k(t) = \alpha k S_k(t)\Theta(t) - (\beta + d)E_k(t), \\ \dot{I}_k(t) = \beta E_k(t) - (\omega + d + \mu + v_k(t))I_k(t), \\ \dot{R}_k(t) = (\omega + v_k(t))I_k(t) - (\delta + d)R_k(t). \end{cases} \tag{4.1}$$

In this formulation, $v_k(t)I_k(t)$ captures the policy-induced transition rate from active distress to the restructured/resilient state, augmenting the system's endogenous recovery capacity.

The regulator seeks to balance the social cost of operational disruptions against the fiscal burden of the intervention. We define the objective functional $J(\boldsymbol{v})$ over the planning horizon $[0, T]$ as

$$J(\boldsymbol{v}) = \int_0^T \sum_{k=1}^{n} \left[L_k I_k(t) + \frac{1}{2} B_k v_k^2(t) \right] \mathrm{d}t, \tag{4.2}$$

where L_k (normalized to 1 here) represents the systemic loss per distressed unit, and $B_k > 0$ denotes the marginal cost of implementing a stimulus for degree-k suppliers. The quadratic form of the control cost captures convex adjustment costs and the increasing difficulty of scaling interventions under diminishing returns.

Theorem 4.1 (Existence of an optimal policy)**.** *Given the controlled system* (4.1)*, there exists an optimal control trajectory $\boldsymbol{v}^* \in \mathbb{V}$ such that $J(\boldsymbol{v}^*) = \inf_{\boldsymbol{v} \in \mathbb{V}} J(\boldsymbol{v})$.*

Proof. The existence of an optimal control is established by verifying the Filippov-Cesari requirements for the Bolza problem [46]:

(i) The admissible set $\mathbb{V}$ is a closed, bounded, and convex subset of $L^\infty(0,T;\mathbb{R}^n)$. By the Banach-Alaoglu theorem, it is weakly compact.
(ii) The right-hand side of (4.1) is Lipschitz continuous with respect to the state variables (S,E,I,R) and affine in the control $\boldsymbol{v}$. For any $\boldsymbol{v}\in\mathbb{V}$, the Carathéodory conditions are satisfied, ensuring the existence of a unique, bounded solution on $[0,T]$.
(iii) As established in Lemma 2.2, the state trajectories remain in the compact, positively invariant simplex $\Omega\subset\mathbb{R}^{4n}_+$. This uniform boundedness prevents finite-time blow-up.
(iv) The running cost $\mathcal{L}(\mathbf{x},\mathbf{v}) = \sum(I_k + \frac{1}{2}B_k v_k^2)$ is continuous in $\mathbf{x}$ and strictly convex in $\mathbf{v}$ (since $\nabla_v^2\mathcal{L} = \mathrm{diag}(B_k) \succ 0$). This ensures the lower semi-continuity of the objective functional in the weak topology.

Since all conditions for the existence of an optimal solution in a bounded domain are satisfied, there exists a $\boldsymbol{v}^*\in\mathbb{V}$ that achieves the minimum social cost. □

To derive the optimal intervention strategy $\boldsymbol{v}^*(t)$ that minimizes the social cost functional $J(\boldsymbol{v})$, we apply Pontryagin's minimum principle [46, 47]. This principle provides the necessary conditions for optimality by transforming the dynamic optimization problem into a pointwise minimization of the Hamiltonian.

Define the Hamiltonian $\mathcal{H}$ for the controlled system (4.1) as follows:

$$\mathcal{H}(t) = \sum_{k=1}^{n}\left[I_k(t) + \frac{1}{2}B_k v_k^2(t)\right] + \sum_{k=1}^{n}\sum_{i\in\{S,E,I,R\}}\lambda_{ik}(t)f_{ik}(\mathbf{x},\boldsymbol{v}), \tag{4.3}$$

where $\lambda_{ik}(t)$ are the adjoint (costate) variables associated with each state i in degree class k, and f_{ik} represents the corresponding vector field from system (4.1). The costate variables function as shadow prices, representing the marginal change in the objective functional with respect to a marginal shift in the enterprise population states.

Theorem 4.2 (Optimal policy characterization)**.** *Let $\mathcal{O}^*(t) = \{S_k^*, E_k^*, I_k^*, R_k^*\}_{k=1}^n$ be the optimal state trajectories. Then there exist adjoint variables $\lambda_{ik}(t)$ satisfying the following system of differential equations:*

$$\dot{\lambda}_{ik}(t) = -\frac{\partial\mathcal{H}}{\partial x_{ik}}, \quad \lambda_{ik}(T) = 0, \quad \forall i\in\{S,E,I,R\}, \quad \forall k. \tag{4.4}$$

Specifically, the adjoint dynamics for each degree class k are given by

$$\begin{aligned}
\dot{\lambda}_{Sk} &= (\lambda_{Sk} - \lambda_{Ek})\alpha k\Theta^*\left(1 - \frac{S_k^*}{N_k^*}\right) + d\lambda_{Sk},\\
\dot{\lambda}_{Ek} &= (\lambda_{Ek} - \lambda_{Sk})\alpha k\Theta^*\frac{S_k^*}{N_k^*} + (\beta + d)\lambda_{Ek} - \beta\lambda_{Ik},\\
\dot{\lambda}_{Ik} &= -1 + (\lambda_{Sk} - \lambda_{Ek})\alpha k S_k^*\Theta^*\frac{1}{N_k^*}\left(1 - \frac{I_k^*}{N_k^*}\right) + (\omega + d + \mu + v_k^*)\lambda_{Ik} - (\omega + v_k^*)\lambda_{Rk},\\
\dot{\lambda}_{Rk} &= (\lambda_{Ek} - \lambda_{Sk})\alpha k\Theta^*\frac{S_k^*}{N_k^*} - \delta\lambda_{Sk} + (\delta + d)\lambda_{Rk}.
\end{aligned}$$

The optimal recovery-stimulus intensity $v_k^*(t)$ for each connectivity stratum k is characterized by the saturation formula

$$v_k^*(t) = \max\left\{0, \min\left(1, \frac{(\lambda_{Ik}(t) - \lambda_{Rk}(t))I_k^*(t)}{B_k}\right)\right\}. \tag{4.5}$$

Proof. According to the Pontryagin minimum principle, the optimal control $\boldsymbol{\nu}^*$ must minimize $\mathcal{H}$ pointwise over the admissible set $\mathbb{V} = [0,1]^n$. The adjoint equations (4.4) are derived from the first-order necessary conditions $\dot{\lambda} = -\nabla_{\mathbf{x}}\mathcal{H}$.

A critical complexity in the differentiation arises from the network interaction term

$$\Theta(t) = \frac{1}{\langle k\rangle}\sum kP_k\frac{I_k}{N_k}.$$

Note that for a specific degree class k, the partial derivatives are

$$\frac{\partial\Theta}{\partial S_k} = \frac{\partial\Theta}{\partial E_k} = \frac{\partial\Theta}{\partial R_k} = -\frac{1}{\langle k\rangle}\frac{kP_kI_k}{N_k^2} = -\frac{\Theta}{N_k}, \quad \frac{\partial\Theta}{\partial I_k} = \frac{1}{\langle k\rangle}\frac{kP_k(N_k - I_k)}{N_k^2} = \frac{\Theta}{I_k}\left(1 - \frac{I_k}{N_k}\right).$$

Substituting these into the gradient of the Hamiltonian (4.3) with respect to the state variables yields the adjoint system. The transversality condition $\lambda_{ik}(T) = 0$ follows from the absence of a terminal cost in the objective functional.

To find the optimal control, we examine the optimality condition $\partial\mathcal{H}/\partial v_k = 0$ and obtain

$$\frac{\partial\mathcal{H}}{\partial v_k} = B_kv_k - \lambda_{Ik}I_k + \lambda_{Rk}I_k = 0 \implies v_k = \frac{(\lambda_{Ik} - \lambda_{Rk})I_k}{B_k}.$$

Since $v_k(t)$ is constrained to the interval $[0,1]$, the optimal trajectory is obtained by projecting this candidate onto the admissible set, resulting in the threshold-based policy (4.5). □

Remark 7. *In Theorem 4.2, the term $\lambda_{Ik} - \lambda_{Rk}$ represents the marginal social benefit of moving a firm from the infected state to the recovered state, i.e., the shadow price of recovery. The optimal policy $v_k^*(t)$ is a saturation rule: full stimulus ($v_k = 1$) is applied when this benefit exceeds the unit cost B_k; no stimulus ($v_k = 0$) is applied when the benefit is negative or negligible. The intensity scales linearly with I_k, meaning a larger number of currently distressed firms in degree class k warrants stronger intervention, all else being equal. Regarding degree heterogeneity, high-degree firms contribute disproportionately to network-wide contagion via $\Theta(t)$, leading to larger shadow prices. Consequently, higher-degree firms should receive stronger or earlier stimulus, a result consistent with targeted immunization strategies in network epidemiology. This dynamic, hub-prioritizing rule enables precise, budget-efficient risk flattening by linking intervention intensity to real-time systemic valuation, thereby avoiding indiscriminate bailouts.*

5. Numerical simulations

To elucidate the contagion dynamics and the effectiveness of the proposed control strategies, we perform extensive numerical simulations of the degree-resolved SEIRS system (2.1). The primary objectives are to validate the threshold theory surrounding the basic reproduction number $\mathcal{R}_0$ and to quantify the sensitivity of systemic risk to both topological parameters and intervention intensities.

5.1. Scale-free network results

Reflecting the empirical architecture of global supply chains, characterized by a small number of highly connected hub enterprises and a vast periphery of smaller suppliers, we ground our analysis in a heterogeneous scale-free network topology. Such structures are governed by the Barabási-Albert paradigm, where the degree distribution follows the power law

$$P_k = \zeta k^{-\gamma}, \quad k = 1, 2, \ldots, n,$$

with an exponent $\gamma = 3$ and a maximum degree (cut-off) of $n = 30$. Solving the normalization condition $\sum_{k=1}^{n} P_k = 1$ yields the scaling constant $\zeta \approx 0.8323$. This configuration yields the following statistical moments:

$$\langle k \rangle = \sum_{k=1}^{n} kP_k \approx 1.3418, \quad \langle k^2 \rangle = \sum_{k=1}^{n} k^2 P_k \approx 3.3249.$$

The resulting heterogeneity ratio, $\langle k^2 \rangle / \langle k \rangle \approx 2.48$, serves as a critical multiplier for risk cascades, representing a stringent test-bed for our resilience analysis. To monitor the macro-state of the network, we define the network-wide densities (ensemble averages) as

$$X(t) = \sum_{k=1}^{n} P_k X_k(t), \quad X \in \{S, E, I, R\}. \tag{5.1}$$

These aggregated variables represent the expected fraction of enterprises in each risk state across the entire supply chain.

In this study, we normalize the total population such that the carrying capacity of the system in the distress-free state is unity (i.e., $N_k^0 = 1$). Accordingly, we set the entry rate $b = 0.3$ and the natural exit (attrition) rate $d = 0.3$. This calibration ensures that $S_k \to b/d = 1$ in the absence of risk, allowing us to interpret the state variables as relative densities or market shares. The remaining parameters are calibrated based on existing literature in supply chain risk and financial contagion (see Table 2).

Table 2. Baseline parameter calibration for the SEIRS system (2.1).

Parameter	Description	Value	Economic/Analytic Justification	Source
b	Market Entry Rate	0.3	Normalized such that $b/d = 1$	[48]
d	Natural Attrition Rate	0.3	Structural turnover of firms	[49]
α	Transmission Intensity	0.6	Contagion strength across business ties	[30, 50]
β	Latency Transition Rate	0.5	Rate of latent risk manifesting as distress	[51, 52]
ω	Recovery/Elasticity Rate	0.05	Speed of restructuring and re-sourcing	[52, 53]
μ	Risk-Induced Failure	0.1	Excess bankruptcy rate under distress	[49]
δ	Immunity Decay Rate	0.2	Rate of recovered firms becoming re-vulnerable	[49]

To bridge the mathematical formulation with operational realities, the baseline parameters in Table 2 are interpreted as follows. The transmission intensity $\alpha = 0.6$ implies that a distressed firm has a 60% probability of infecting each of its direct business partners per unit time. The latency transition rate $\beta = 0.5$ gives an average incubation period of $1/\beta = 2$ time units, which may represent, for example, the two-week lag between a supplier's initial production hiccup and observable downstream

shortages. The recovery rate $\omega = 0.05$ corresponds to an expected downtime of $1/\omega = 20$ time units. In practice, this could translate to a six-month capacity ramp-up following a major disruption (e.g., post-COVID semiconductor reallocation or port closure recovery). The risk-induced failure rate $\mu = 0.1$ indicates that 10% of manifestly distressed firms exit the market per time unit, capturing bankruptcy cascades seen in events like the 2011 Thai floods or the 2020–2021 automotive chip crisis. Finally, the immunity decay rate $\delta = 0.2$ means that a recovered firm becomes re-vulnerable after $1/\delta = 5$ time units on average, mirroring the gradual erosion of buffer stocks, contract renegotiations, or supplier switching, a phenomenon often observed in fast-turnover industries such as fast-moving consumer goods or electronics assembly.

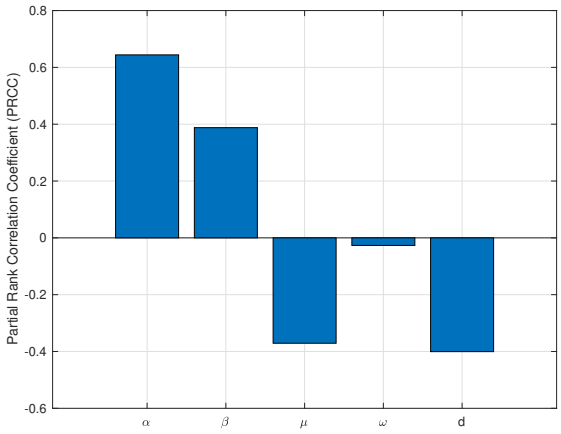

Figure 2. Sensitivity of the basic reproduction number $\mathcal{R}_0$ to parameter variation.

Figure 2 presents the partial rank correlation coefficient (PRCC) results, which aim to quantitatively identify the global sensitivity strength and dominant ranking of multiple endogenous and exogenous parameters affecting the systemic risk threshold $\mathcal{R}_0$. This global sensitivity screening clarifies which network topological parameters and contagion parameters play core leading roles in regulating the overall risk contagion scale. The results indicate that α (contagion intensity) and β (latency transition rate) exhibit the most significant positive correlations with $\mathcal{R}_0$. This suggests that the systemic threshold is highly sensitive to the efficacy of risk transmission across business ties and the prolonged duration of latent vulnerability, both of which expand the contagion window within the network. Conversely, the structural parameters μ (risk-induced bankruptcy) and d (market attrition) display substantial negative PRCC values. These results underscore that the metabolic clearing of distressed nodes, facilitated by swift insolvency proceedings or market delisting, effectively curtails the infectious duration, thereby suppressing the potential for a self-sustaining cascade. The restorative capacity ω (internal risk management) sits in a moderate position, implying that while enhancing recovery protocols is beneficial, its marginal impact on dampening $\mathcal{R}_0$ is secondary to ex-ante containment or ex-post structural removal.

Synthetically, the sensitivity landscape advocates for a contain-and-clear policy regime. To achieve the most significant reduction in systemic risk, managers and regulators should prioritize ex-ante structural decoupling (e.g., implementing multi-sourcing to reduce α) and ex-post rigorous auditing (e.g., accelerating the write-off of insolvent entities to increase μ and d) over purely reactive restorative efforts.

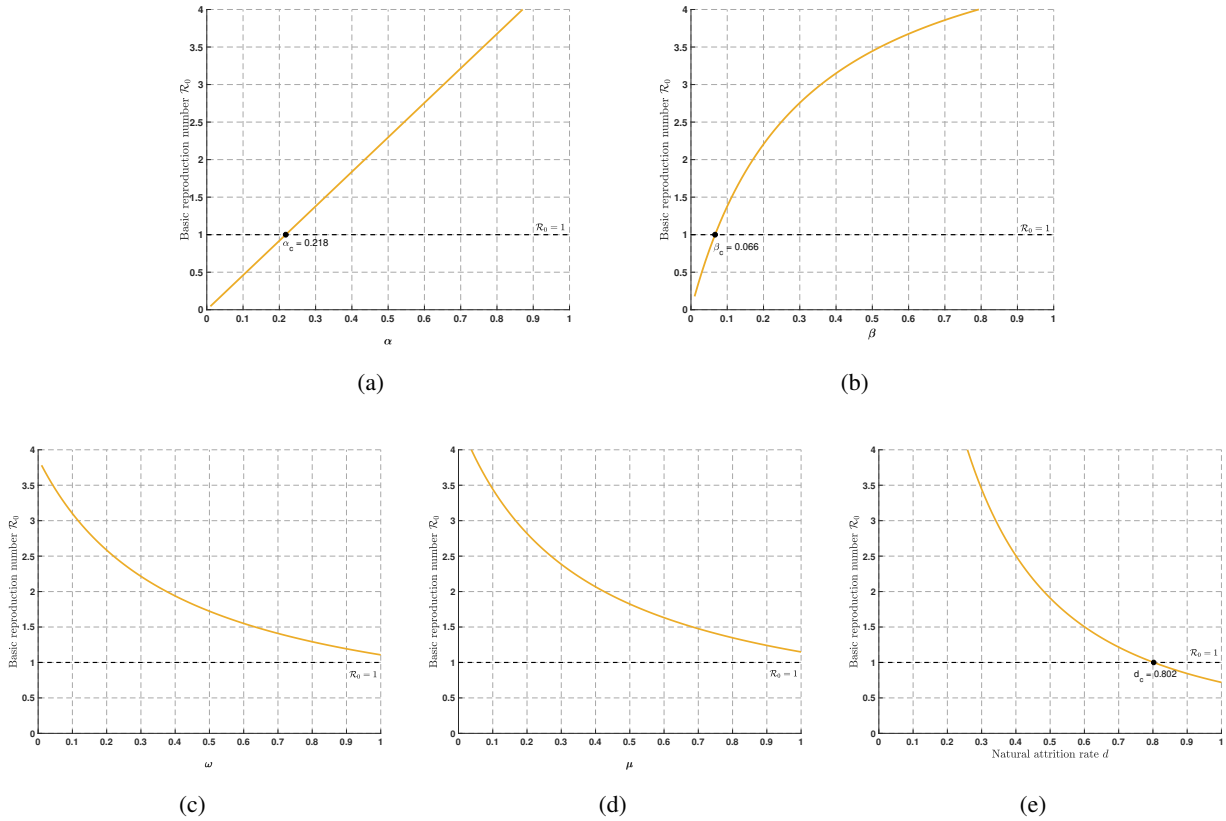

Figure 3. Sensitivity of the basic reproduction number $\mathcal{R}_0$ to (a) risk transmission rate α, (b) risk conversion rate β, (c) recovery capability ω, (d) market-elimination rate μ, and (e) firm-exit rate d. All other parameters are given in Table 2.

Figure 3 further complements and extends the results of Figure 2 by focusing on the local dynamic response characteristics. It separately reveals the monotonic changing trend of the critical threshold $\mathcal{R}_0$ under continuous single-parameter perturbation, which verifies the independent influence mechanism of key sensitive parameters on the phase transition boundary of supply chain systemic risk.

As shown in Figure 3(a), the risk contagion rate α (representing the probability of contagion between firms) has a positive influence. This confirms that structural connectivity and the intensity of disruptive contagion are the primary drivers of system cascading. Similarly, Figure 3(b) shows that the conversion rate β is positively correlated with $\mathcal{R}_0$, suggesting that accelerating early detection and internal audits to shorten the incubation period can serve as an effective secondary defense mechanism. Conversely, Figure 3(c) shows an inverse relationship between $\mathcal{R}_0$ and the recovery rate ω. Enhancing firms' self-repair capabilities through strategic inventory buffers, dual-source financing, or government liquidity support can effectively mitigate contagion risk. Furthermore, Figures 3(d) and 3(e) show that increasing the market attrition rate μ and the firm exit rate d reduces $\mathcal{R}_0$. By accelerating the elimination of distressed firms, the network can effectively purge potential spreaders, thereby controlling risk. These results indicate that strong network resilience cannot rely solely on firm exit policies; instead, it requires a prioritized intervention strategy that emphasizes ex-ante control of contagion (α) and ex-post accelerated recovery (ω).

To conduct the sensitivity analysis, we vary each of the three key parameters (α, β, and ω) individually within ±30% of their baseline values, while holding all other parameters fixed at the values reported in Table 2. Table 3 summarizes the resulting minimum and maximum values for each parameter. For each parameter, we compute $\mathcal{R}_0$ across 100 equally spaced points within this range using the analytical expression $\mathcal{R}_0 = \frac{\langle k^2 \rangle}{\langle k \rangle} \cdot \frac{\alpha\beta}{(\beta+d)(\omega+d+\mu)}$, with the network heterogeneity ratio fixed at the scale-free network value $\langle k^2 \rangle / \langle k \rangle = 2.48$.

Table 3. Parameter ranges for sensitivity analysis.

Parameter	Baseline	Min	Max	Variation
α	0.6	0.42	0.78	±30%
β	0.5	0.35	0.65	±30%
ω	0.05	0.035	0.065	±30%

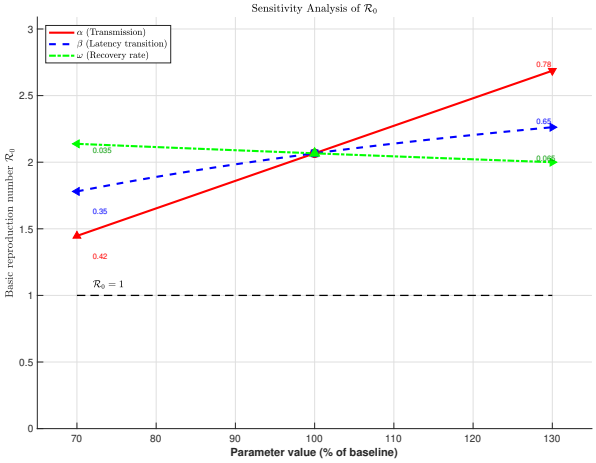

Figure 4. Sensitivity analysis of the basic reproduction number $\mathcal{R}_0$ with respect to the three key parameters: α (transmission intensity), β (latency transition rate), and ω (recovery rate). Each parameter is varied individually within ±30% of its baseline value (marked by a vertical dashed line at 100%), while the other two parameters are held constant at their baselines ($\alpha = 0.6, \beta = 0.5, \omega = 0.05$). The horizontal dashed line indicates the critical threshold $\mathcal{R}_0 = 1$.

Figure 4 shows the sensitivity of $\mathcal{R}_0$ to variations in α, β, and ω. It illustrates how $\mathcal{R}_0$ responds to variations in each parameter. $\mathcal{R}_0$ increases linearly with α and β, while decreasing monotonically with ω, consistent with the analytical expression. Across all parameter variations within the ±30% range, $\mathcal{R}_0 > 1$ holds for the scale-free network, confirming that the endemic state is robust to reasonable parameter uncertainty.

Figure 5 delineates the convergence dynamics of systemic risk prevalence $I(t)$ under two contrasting threshold regimes, normalized such that $I(t)$ quantifies the fraction of the network in distress. With parameters yielding a subcritical basic reproduction number $\mathcal{R}_0 < 1$ (Figure 5(a)), any initial disturbance dissipates rapidly, and damping through recovery and attrition exceeds contagion pressure, driving $I(t)$ to zero without external intervention. Conversely, for $\mathcal{R}_0 > 1$ (Figure 5(b)), initial overshoots

settle into a persistent endemic equilibrium, revealing a self-sustaining failure loop that chronically impairs network capacity. These regimes articulate a policy hierarchy: below-threshold conditions permit passive resilience, while above-threshold dynamics necessitate active, targeted mitigation to break the contagion cycle.

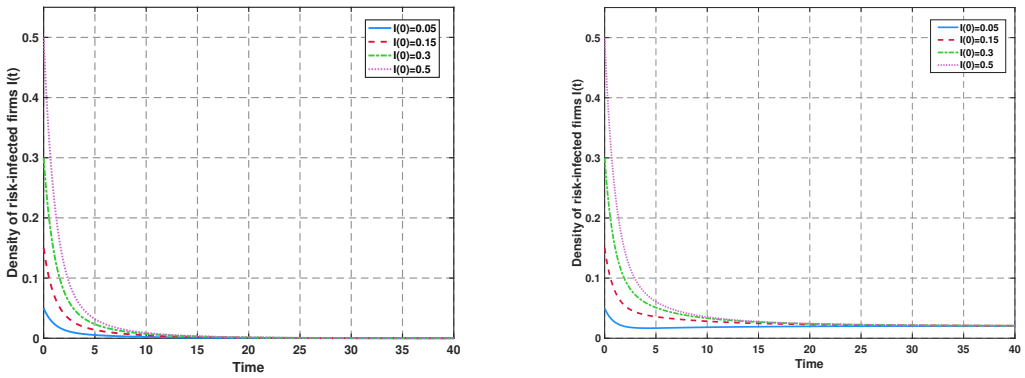

(a) $\mathcal{R}_0 = 0.6195 < 1$ (b) $\mathcal{R}_0 = 1.3939 > 1$

Figure 5. Phase-transition dynamics of the risk-infected density $I(t)$ across varying initial conditions. (a) Convergence to the distress-free equilibrium under $\mathcal{R}_0 < 1$ with $\alpha = 0.4$. (b) Convergence to the endemic equilibrium under $\mathcal{R}_0 > 1$ with $\alpha = 0.9$. The rest of the parameter values are given in Table 2.

5.2. Comparative analysis across network topologies

The preceding numerical analysis has focused exclusively on scale-free networks, which capture the heavy-tailed degree distribution observed in many real-world supply chains. However, empirical supply chain networks often exhibit richer topological features beyond pure scale-free characteristics, including hierarchical structures (multi-tier supplier relationships), modular organization (industrial clusters), and relatively homogeneous connectivity among small-to-medium enterprises. To demonstrate the robustness of our theoretical framework across diverse network architectures and to better align the numerical validation with empirical observations, we extend our investigation to two additional canonical network models: random networks (Erdős-Rényi) and small-world networks (Watts-Strogatz). Figure 6 provides schematic visualizations of these three topologies, highlighting their distinct structural properties.

Figure 6 provides schematic visualizations of the three canonical network models employed in our numerical comparative analysis. Figure 6(a) depicts an Erdős-Rényi random network, where edges exist independently with uniform probability, yielding a Poisson degree distribution. This topology exhibits no dominant hubs and minimal clustering, serving as a homogeneous baseline. Figure 6(b) illustrates a Watts-Strogatz small-world network, constructed by randomly rewiring a fraction $p = 0.1$ of edges from a regular ring lattice. The resulting structure preserves high local clustering (modularity) while introducing a small number of long-range shortcut connections that dramatically reduce the average path length. This topology captures the hierarchical and modular characteristics frequently observed in empirical supply chains, where firms cluster within industrial sectors or geographical regions yet maintain cross-sector linkages through logistics or financial intermediaries. Figure 6(c)

shows a scale-free network generated via the Barabási-Albert preferential attachment mechanism, where new nodes preferentially connect to existing nodes with higher degrees. This process yields a power-law degree distribution $P(k) \sim k^{-\gamma}$ with $\gamma = 3$ in our configuration, characterized by a small number of high-degree hub nodes (visually prominent in the figure) and a large number of low-degree peripheral nodes. The topological distinction among these models directly translates into differential risk contagion dynamics as quantified in Figure 7, underscoring the importance of topology-aware risk management.

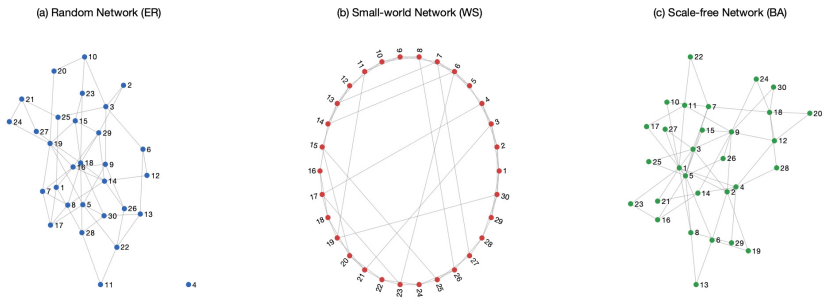

Figure 6. Schematic illustrations of the three network topologies used in the comparative analysis. (a) Random network (Erdős-Rényi) with homogeneous degree distribution; (b) small-world network (Watts-Strogatz) with high clustering and short average path length ($p = 0.1$); (c) scale-free network (Barabási-Albert) characterized by a few high-degree hub nodes and many low-degree peripheral nodes ($\gamma = 3$).

Table 4. Topological characteristics of the three network models used for comparative analysis.

Topology	Degree Distribution	Key Parameters	$\langle k \rangle$	$\langle k^2 \rangle / \langle k \rangle$
Scale-free (SF)	$P_k = \zeta k^{-\gamma}$	$\gamma = 3,\ n = 30$	1.34	2.48
Random (ER)	$P_k = \mathrm{e}^{-\langle k \rangle} \langle k \rangle^k / k!$	$\langle k \rangle = 4$	4.00	4.25
Small-world (WS)	Rewired from regular lattice	$p = 0.1,\ \langle k \rangle = 4$	4.00	4.30

Note: SF = scale-free; ER = Erdős-Rényi; WS = Watts-Strogatz. The heterogeneity ratio $\langle k^2 \rangle / \langle k \rangle$ quantifies the vulnerability amplification from hub nodes.

The topological differences illustrated in Figure 6 are quantitatively characterized by the degree distribution statistics reported in Table 4. Notably, while the random and small-world networks share the same average degree $\langle k \rangle = 4$, the scale-free network exhibits a lower $\langle k \rangle = 1.34$ but a distinct heterogeneity ratio $\langle k^2 \rangle / \langle k \rangle = 2.48$, which critically modulates the risk contagion threshold.

Based on the topological parameters in Table 4, Figure 7 illustrates the relationship between the basic reproduction number $\mathcal{R}_0$ and the steady-state risk prevalence $E^* + I^*$, where E^* and I^* denote the equilibrium proportions of latent and infectious enterprises, respectively, as defined in the SEIRS compartmental system (2.1). The vertical dashed line at $\mathcal{R}_0 = 1$ delineates the transcritical bifurcation point derived from our heterogeneous mean-field analysis. This threshold is universal across all network topologies: when $\mathcal{R}_0 < 1$, initial disturbances decay exponentially, and the system converges to the risk-free equilibrium ($E^* + I^* = 0$); when $\mathcal{R}_0 > 1$, a unique globally attractive endemic equilibrium emerges, signaling chronic systemic vulnerability.

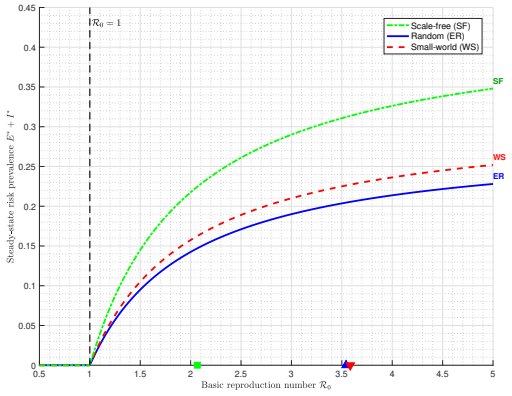

Figure 7. Steady-state risk prevalence $E^* + I^*$ (proportion of latent and infectious enterprises) as a function of the basic reproduction number $\mathcal{R}_0$ for scale-free (SF), small-world (WS), and random (ER) networks. The vertical dashed line marks the transcritical bifurcation threshold $\mathcal{R}_0 = 1$. For $\mathcal{R}_0 < 1$, all topologies converge to the risk-free equilibrium; for $\mathcal{R}_0 > 1$, the scale-free network exhibits the highest prevalence due to hub-driven amplification quantified by the heterogeneity ratio $\langle k^2 \rangle / \langle k \rangle \approx 2.48$.

Above the threshold, the steady-state prevalence increases monotonically with $\mathcal{R}_0$. Notably, the scale-free network exhibits the highest prevalence across the entire $\mathcal{R}_0 > 1$ domain, despite having the smallest average degree ($\langle k \rangle = 1.34$). This counterintuitive phenomenon is directly attributable to the heterogeneity ratio $\langle k^2 \rangle / \langle k \rangle \approx 2.48$, which serves as a network heterogeneity amplifier, i.e., a small fraction of high-degree hub enterprises disproportionately amplifies transmission potential. In contrast, small-world and random networks, with their more homogeneous degree distributions (both exhibiting $\langle k^2 \rangle / \langle k \rangle \approx 4.25$–$4.30$), yield substantially lower steady-state prevalence levels.

The computed $\mathcal{R}_0$ values (ER: ≈ 3.54, WS: ≈ 3.58, SF: ≈ 2.07) reveal that random and small-world networks exhibit higher theoretical transmission potential than the scale-free configuration under our parameter calibration. However, as shown in Figure 7, the scale-free network ultimately attains a higher steady-state prevalence due to hub-driven amplification. This apparent paradox establishes three insights: (i) the threshold $\mathcal{R}_0 = 1$ is universal; (ii) vulnerability is not fully determined by $\mathcal{R}_0$; and (iii) heavy-tailed structures are intrinsically more fragile once the risk surpasses the threshold.

5.3. Optimal control analysis

Figure 8 depicts the transition from contagion dominance to intervention-driven recovery as a function of risk-control intensity v_k, with the network normalized by setting the entry rate equal to the attrition rate ($b = d$), so that $S(t)$ and $I(t)$ represent densities of resilient and distressed firms. For low intervention ($v_k \to 0$), the system enters a contagion trap: $S(t)$ collapses and remains suppressed, while $I(t)$ rises to a high endemic level, indicating that risk contagion overwhelms endogenous recovery. Increasing v_k shifts the equilibrium: $S(t)$ displays a V-shaped rebound, and $I(t)$ peaks earlier and decays toward zero. This highlights how targeted stimulus curtails the disruption window by accelerating the restructuring of distressed firms, thereby starving the contagion and restoring systemic resilience.

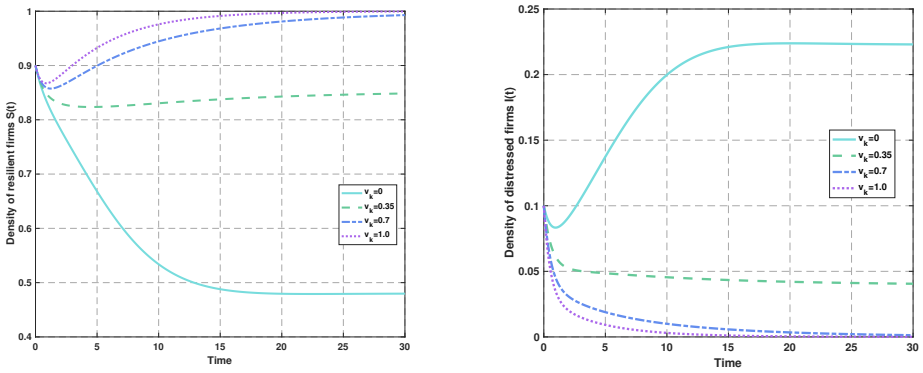

(a) Change in healthy-firm $S(t)$ with varying the risk-control intensity

(b) Change in risk-infected firm $I(t)$ with varying the risk-control intensity

Figure 8. Temporal evolution of ensemble-averaged densities for resilient (S) and distressed (I) enterprises under control efforts v_k. The other fixed parameter values are the same as in Table 2.

Figure 9 delineates the non-monotonic landscape of the aggregate social cost functional $J(v_k)$, elucidating the fundamental inter-temporal trade-off between operational risk truncation and fiscal sustainability. In this normalized framework ($b = d$), the objective function J serves as a proxy for the total socioeconomic burden, comprising two antagonistic components: the cumulative systemic distress, represented by the integral of infected density $I(t)$, and the convex expenditure associated with intervention outlays. At the lower bound of control ($v_k \to 0$), the network remains in a contagion-dominated regime where passive governance allows risk cascades to permeate the topology unhindered, resulting in maximal social loss despite zero fiscal spending. Conversely, as the recovery stimulus v_k is scaled, the system undergoes a transition toward an intervention-led recovery; however, the quadratic nature of control costs implies diminishing marginal returns.

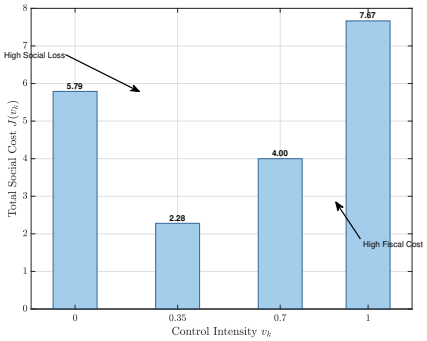

Figure 9. The total cost objective function ($J(v_k)$) versus the risk-control intensity (v_k). All other parameters are given in Table 2.

The existence of a global minimum in Figure 9 confirms that the optimal regulatory policy is neither total passivity nor indiscriminate bailouts, but a targeted stimulus that identifies a threshold where the marginal utility of risk reduction precisely balances the escalating marginal cost of public assistance.

This numerical validation reinforces the necessity of dynamic optimal control in managing network externalities within complex supply chain ecosystems.

6. Conclusions

This study elucidates the systemic dynamics of risk contagion and regulatory stabilization within heterogeneous supply chain networks. By integrating the heterogeneous mean-field framework with an SEIRS compartmental structure, we characterize the evolutionary life cycle of disruptions from latent absorption and manifest functional failure to restorative restructuring and subsequent resilience decay.

Our analytical results identify the basic reproduction number $\mathcal{R}_0$ as a criterion for systemic collapse. Specifically, the network resides in a self-healing regime when $\mathcal{R}_0 < 1$, where localized perturbations dissipate asymptotically. Conversely, for $\mathcal{R}_0 > 1$, the system undergoes a bifurcation, settling into a persistent endemic risk regime where operational distress permeates every connectivity stratum. Sensitivity analysis reveals that systemic fragility is significantly amplified by the manifestation lag (the duration of latent vulnerability) and the erosion of restructured buffers ($R \to S$). While natural attrition and market clearing provide a passive metabolic damping for risk, the implementation of a targeted stimulus is shown to be essential for shifting the system from a contagion-dominated trap to an intervention-led recovery.

Synthesizing these findings, we offer the following strategic insights for systemic risk governance:

(1) Risk-mitigation policies must prioritize the fortification of high-degree hub enterprises, as their connectivity acts as a multiplier for systemic cascades. Given their weight in the determination of $\mathcal{R}_0$, targeted investments in their redundancy and endogenous restorative capacity (e.g., dual-sourcing and capital liquidity) yield superior returns in reducing the systemic contagion threshold compared to uniform network-wide assistance.
(2) Managers should transition from reactive firefighting to a proactive early-warning regime anchored in the real-time monitoring of the latent-to-infectious manifestation rate. By accelerating the detection of hidden shocks (state E) and decoupling counterparty exposures before operational failures (state I) materialize, the organization can truncate the infectious window and prevent localized disruptions from achieving self-sustaining momentum.
(3) Regulatory intervention should be framed as a dynamic optimization problem that balances risk suppression against fiscal sustainability. The observed U-shaped social cost functional $J(v_k)$ implies that the optimal policy resides at a Pareto-efficient threshold. Decision-makers should avoid the traps of both passive neglect and indiscriminate over-leveraging, instead deploying degree-aware stimuli that achieve the maximal marginal reduction in systemic distress per unit of fiscal outlay.

A limitation of our modeling framework is the instantaneous replacement assumption, which posits that exiting firms are immediately replaced by new entrants with identical degree centrality. While this assumption is standard in mean-field epidemic models for mathematical tractability and population closure, it may introduce a systematic bias toward underestimating the cumulative effect of systemic risk. Specifically, by eliminating replacement delays and ignoring the difficulty of restoring hub nodes after failure, the model likely produces a lower bound on steady-state infection prevalence rather than an exact prediction. Importantly, however, the qualitative threshold $\mathcal{R}_0 = 1$ and the comparative ranking of intervention strategies remain robust, as both depend primarily on network heterogeneity

captured by $\langle k^2\rangle/\langle k\rangle$ rather than on replacement timing. Given this limitation, future research should relax the instantaneous replacement assumption by incorporating explicit time delays for market entry, endogenous network reconfiguration following firm exits, and degree-dependent replacement probabilities that reflect the difficulty of substituting high-degree hub suppliers. Such extensions would provide a more accurate assessment of systemic risk accumulation in supply chains characterized by high asset specificity, long qualification cycles, or concentrated supplier bases.

Use of Generative-AI tools declaratio

The authors declare that they did not utilize any artificial intelligence (AI) tools in the creation of this manuscript.

Author contributions

Shufen Wei: Writing–original draft, Visualization. Yannan Su: Writing–original draft, Visualization. Shufen Wei and Yannan Su: contributed equally to this work. Zhanyu Wang: Writing–review and editing, Visualization. Xinze Lian: Visualization. Feng Rao: Writing–review and editing, Validation, Supervision, Methodology, Conceptualization. All authors have read and agreed to the published version of the manuscript.

Acknowledgements

This work is partially supported by the Qing Lan Project of Jiangsu Province and Project of Philosophy and Social Science Research in Colleges and Universities in Jiangsu Province (2021SJB0081), as well as the Zhejiang Provincial Natural Science Foundation of China under Grant LZ23A010003.

Conflict of interest

The authors declare no conflicts of interest.

Data availability

There are no data associated in the manuscript.

References

1. T. Y. Choi, K. J. Dooley, M. Ruangtusanathan, Supply networks and complex adaptive systems: control versus emergence, *J. Oper. Manag.,* **19** (2001), 351–366. https://doi.org/10.1016/S0272-6963(00)00068-1
2. A. Surana, S. Kumara, M. Greaves, U. Raghavan, Supply-chain networks: a complex adaptive systems perspective, *Int. J. Prod. Res.,* **43** (2005), 4235–4265. https://doi.org/10.1080/00207540500142274

3. D. Ivanov, *Structural dynamics and resilience in supply chain risk management,* Springer Cham, 2018. https://doi.org/10.1007/978-3-319-69305-7
4. Y. H. Li, K. D. Chen, S. Collignon, D. Ivanov, Ripple effect in the supply chain network: forward and backward disruption propagation, network health and firm vulnerability, *Eur. J. Oper. Res.,* **291** (2021), 1117–1131. https://doi.org/10.1016/j.ejor.2020.09.053
5. J. P. Wang, H. Zhou, X. D. Jin, Risk transmission in complex supply chain network with multi-drivers, *Chaos Solit. Fract.,* **143** (2021), 110259. https://doi.org/10.1016/j.chaos.2020.110259
6. A. Dolgui, D. Ivanov, M. Rozhkov, Does the ripple effect influence the bullwhip effect? An integrated analysis of structural and operational dynamics in the supply chain, *Int. J. Prod. Res.,* **58** (2020), 1285–1301. https://doi.org/10.1080/00207543.2019.1627438
7. N. O. Hohenstein, Supply chain risk management in the COVID-19 pandemic: strategies and empirical lessons for improving global logistics service providers' performance, *Int. J. Logist. Manag.,* **33** (2022), 1336–1365. https://doi.org/10.1108/IJLM-02-2021-0109
8. A. Świerczek, The impact of supply chain integration on the "snowball effect" in the transmission of disruptions: An empirical evaluation of the model, *Int. J. Prod. Econ.,* **157** (2014), 89–104. https://doi.org/10.1016/j.ijpe.2013.08.010
9. D. J. Watts, A simple model of global cascades on random networks, *PNAS,* **99** (2002), 5766–5771. https://doi.org/10.1073/pnas.082090499
10. N. Osadchiy, V. Gaur, S. Seshadri, Systematic risk in supplychain networks, *Manag. Sci.,* **62** (2015), 1755–1777. https://doi.org/10.1287/mnsc.2015.2187
11. Y. H. Li, C. W. Zobel, O. Seref, D. Chatfield, Network characteristics and supply chain resilience under conditions of risk propagation, *Int. J. Prod. Econ.,* **223** (2020), 107529. https://doi.org/10.1016/j.ijpe.2019.107529
12. J. Mei, S. X. Wang, X. H. Xia, W. F. Wang, An economic model predictive control for knowledge transmission processes in multilayer complex networks, *IEEE Trans. Cybern.,* **54** (2024), 1442–1455. https://doi.org/10.1109/TCYB.2022.3204568
13. A. Barabási, R. Albert, Emergence of scaling in random networks, *Science,* **286** (1999), 509–512. https://doi.org/10.1126/science.286.5439.509
14. H. Chen, A. Lin, Complex network characteristics and invulnerability simulating analysis of supply chain, *J. Netw.,* **7** (2012), 591–597. https://doi.org/10.4304/jnw.7.3.591-597
15. T. Kito, K. Ueda, The implications of automobile parts supply network structures: a complex network approach, *CIRP Ann.,* **63** (2014), 393–396. https://doi.org/10.1016/j.cirp.2014.03.119
16. R. C. Basole, M. A. Bellamy, Supply network structure, visibility, and risk diffusion: a computational approach, *Decis. Sci.,* **45** (2014), 753–789. https://doi.org/10.1111/deci.12099
17. H. Wang, T. Gu, M. Z. Jin, R. Zhao, G. X. Wang, The complexity measurement and evolution analysis of supply chain network under disruption risks, *Chaos Solit. Fract.,* **116** (2018), 72–78. https://doi.org/10.1016/j.chaos.2018.09.018
18. R. Wiedmer, S. E. Griffis, Structural characteristics of complex supply chain networks, *J. Bus. Logist.,* **42** (2021), 264–290. https://doi.org/10.1111/jbl.12283

19. T. Sawik, B. Sawik, Risk-averse decision-making to maintain supply chain viability under propagated disruptions, *Int. J. Prod. Res.,* **62** (2024), 2853–2867. https://doi.org/10.1080/00207543.2023.2236726

20. H. W. Hethcote, The mathematics of infectious diseases, *SIAM Rev.,* **42** (2000), 599–653. https://doi.org/10.1137/S0036144500371907

21. R. M. May, S. A. Levin, G. Sugihara, Complex systems: ecology for bankers, *Nature,* **451** (2008), 893–895. https://doi.org/10.1038/451893a

22. X. J. Liu, J. Gao, M. F. He, Risk contagion mechanism and control strategies in supply chain finance using SEIR epidemic model from the perspective of commercial banks, *Mathematics,* **13** (2025), 2051. https://doi.org/10.3390/math13132051

23. Z. M. Lei, M. K. Lim, L. Cui, Y. Z. Wang, Modelling of risk transmission and control strategy in the transnational supply chain, *Int. J. Prod. Res.,* **59** (2021), 148–167. https://doi.org/10.1080/00207543.2019.1698782

24. C. Zheng, Complex network propagation effect based on SIRS model and research on the necessity of smart city credit system construction, *Alex. Eng. J.,* **61** (2022), 403–418. https://doi.org/10.1016/j.aej.2021.06.004

25. K. Y. Liu, Y. X. Xia, C.Y. Xia, H. C. Tu, Impact of heterogeneity on risk propagation in supply chain networks, *Physica A.,* **679** (2025), 131021. https://doi.org/10.1016/j.physa.2025.131021

26. J. P. Wang, H. Zhou, Y. J. Zhao, Behavior evolution of supply chain networks under disruption risk–from aspects of time dynamic and spatial feature, *Chaos Solit. Fract.,* **158** (2022), 112073. https://doi.org/10.1016/j.chaos.2022.112073

27. J. Mei, S. X. Wang, D. Xia, J. H. Hu, Global stability and optimal control analysis of a knowledge transmission model in multilayer networks, *Chaos Solit. Fract.,* **164** (2022), 112708. https://doi.org/10.1016/j.chaos.2022.112708

28. Y. T. Li, Z. M. Tan, C. Y. Huang, Research on risk contagion mechanism of big fintech based on the SIRS model, *PLoS One,* **18** (2023), e0291230. https://doi.org/10.1371/journal.pone.0291230

29. D. Chang, Y. P. Zhang, Y. T. Guo, *A study of green supply chain finance risk contagion measurement based on SEIRS model*, Springer Nature Singapore, 2024, 167–184. https://doi.org/10.1007/978-981-97-4137-3_14

30. L. Jiang, J. X. Liang, Y. F. Yi, D. M. Liu, Risk propagation and intervention in a complex supply chain network under public emergency, *Comput. Ind. Eng.,* **213** (2026), 111797. https://doi.org/10.1016/j.cie.2025.111797

31. A. Barabási, R. Albert, H. Jeong, Mean-field theory for scale-free random networks, *Physica A,* **272** (1999), 173–187. https://doi.org/10.1016/S0378-4371(99)00291-5

32. M. E. J. Newman, The structure and function of complex networks, *SIAM Rev.,* **45** (2003), 167–256. https://doi.org/10.1137/S003614450342480

33. W. Hopp, M. Spearman, *Factory physics,* Waveland Press, 2011.

34. S. Y. Ponomarov, M. C. Holcomb, Understanding the concept of supply chain resilience, *Int. J. Logist. Manag.,* **20** (2009), 214–243. https://doi.org/10.1108/09574090910954873

35. C. S. Tang, Perspectives in supply chain risk management, *Int. J. Prod. Econ.,* **103** (2006), 451–488. https://doi.org/10.1016/j.ijpe.2005.12.006

36. S. P. Sethi, *Optimal control theory: Applications to management science and economics*, Springer, 2019. https://doi.org/10.1007/978-3-030-91745-6

37. H. Mamani, S. Chick, D. Simchi-Levi, A game-theoretic model of international influenza vaccination coordination, *Manag. Sci.,* **59** (2013), 1650–1663. https://doi.org/10.1287/mnsc.1120.1661

38. Y. Moreno, R. Pastor-Satorras, A. Vespignani, Epidemic outbreaks in complex heterogeneous networks, *Eur. Phys. J. B.,* **26** (2002), 521–529. https://doi.org/10.1140/epjb/e20020122

39. R. Yang, B. Wang, J. Ren, W. Bai, Z. Shi, W. Wang, T. Zhou, Epidemic spreading on heterogeneous networks with identical infectivity, *Phys. Lett. A,* **364** (2006), 189–193. https://doi.org/10.1016/j.physleta.2006.01.053

40. S. Vikram, S. Sinha, Emergence of universal scaling in financial markets from mean-field dynamics, *Phys. Rev. E,* **83** (2011), 016101. https://doi.org/10.1103/PhysRevE.83.016101

41. R. Pastor-Satorras, A. Vespignani, Epidemic spreading in scale-free networks, *Phys. Rev. Lett.,* **86** (2001), 3200–3203. https://doi.org/10.1103/PhysRevLett.86.3200

42. P. V. D. Driessche, J. Watmough, Reproduction numbers and sub-threshold endemic equilibria for compartmental models of disease transmission, *Math. Biosci.,* **180** (2002), 29–48. https://doi.org/10.1016/S0025-5564(02)00108-6

43. O. Diekmann, J. Heesterbeek, M. Roberts, The construction of next-generation matrices for compartmental epidemic models, *J. R. Soc. Interface,* **7** (2010), 873–885. https://doi.org/10.1098/rsif.2009.0386

44. H. Song, Q. Li, Decision-making in closed-loop supply chains: effects of government subsidies and risk aversion, *Int. Rev. Financ. Anal.,* **96** (2024), 103566. https://doi.org/10.1016/j.irfa.2024.103566

45. Z. Wang, Z. Jian, X. Ren, Pollution prevention strategies of SMEs in a green supply chain finance under external government intervention, *Environ. Sci. Pollut. Res.,* **30** (2023), 45195–45208. https://doi.org/10.1007/s11356-023-25444-4

46. W. Fleming, R. Rishel, *Deterministic and stochastic optimal control,* Springer Verlag, 1975. https://doi.org/10.1007/978-1-4612-6380-7

47. L. Pontryagin, V. Boltyanskii, R. Gamkrelidze, E. Mischenko, *The Mathematical theory of optimum processes,* New York Wiley, 1962.

48. M. Keeling, P. Rohani, *Modeling infectious diseases in humans and animals,* Princeton University Press, 2008.

49. H. Wang, X. Zhang, Research on supply chain risk transmission mechanism based on improved SIRS model, *Math. Probl. Eng.,* **9** (2022), 9502793. https://doi.org/10.1155/2022/9502793

50. Y. Teng, S. J. Ma, Q. Qian, G. Wang, SEIR-diffusion modeling and stability analysis of supply chain finance based on blockchain technology, *Heliyon,* **10** (2024), e24981. https://doi.org/10.1016/j.heliyon.2024.e24981

51. L. Jiang, J. X. Liang, Risk propagation and intervention in complex supply chain networks during unforeseen public events, *Comput. Eng. Appl.,* **60** (2024), 296–308. https://doi.org/10.3778/j.issn.1002-8331.2306-0327

52. J. B. Broekaert, F. Hafiz, R. Jayaraman, D. L. Torre, Managing resilience and viability of supranational supply chains under epidemic control scenarios, *Omega,* **133** (2024), 103234. https://doi.org/10.1016/j.omega.2024.103234

53. G. Zhao, Y. B. Yang, X. Bao, Dynamic model for the risk spreading in supply chain network and its application, *Syst. Eng. Theory Pract.,* **35** (2015), 2014–2024. https://doi.org/10.12011/1000-6788(2015)8-2014

AIMS Press

© 2026 the Author(s), licensee AIMS Press. This is an open access article distributed under the terms of the Creative Commons Attribution License (https://creativecommons.org/licenses/by/4.0)